Article

Non-invasive action potential recordings using printed electrolyte-gated polymer field-effect transistors

Adrica Kyndiah [1,9] ✉, Giulia Zoe Zemignani [1,2,9], Carlotta Ronchi[1], Gabriele Tullii[1], Aleksandr Khudiakov [3], Giuseppina Iachetta[4], Stefano Chiodini[1], Rosalia Moreddu [4,8], Fabrizio Antonio Viola [1], Peter J. Schwartz [3], Gabriel Gomila[5,6], Francesco De Angelis [4], Luca Sala [3,7] ✉, Maria Rosa Antognazza [1] & Mario Caironi [1] ✉

Scalable and high-throughput platforms to non-invasively record the Action Potentials (APs) of excitable cells are highly demanded to accelerate disease diagnosis and drug discovery. AP recordings are typically achieved with the invasive and low-throughput patch clamp technique. Non-invasive alternatives like planar multielectrode arrays cannot record APs without membrane poration, preventing accurate measurements of disease states and drug effects. Here, we disclose reliable and non-invasive recording of APs with patch clamp-like quality from human stem cell-derived cardiomyocytes using an inkjet-printed polymer semiconductor in an Electrolyte-Gated Field-Effect Transistor configuration. High sensitivity is proven by the detection of drug-induced pro-arrhythmic membrane potential oscillations as early/delayed afterdepolarizations. The higher throughput potential of this platform could significantly enhance disease modelling, drug screening, safety pharmacology and the study of abiotic/biotic interfaces.

Electrophysiology tools are essential for unraveling the electrical activity of cells and tissues, driving advances in cardiology, neuroscience, and drug discovery[1]. Excitable cells, such as myocytes or neurons, exert their function through a complex interplay of ion channels that regulate selective ion fluxes across the membrane. This process generates Action Potentials (APs), which are rapid changes in the trans-membrane voltage that occur spontaneously or triggered by electrical stimuli. The morphology, duration and amplitude of the AP convey relevant information about the physiological state and functional properties of the cell, and specific alterations in the morphology

or in the duration of the AP are clear markers of pathological states[2]. There is a strong need for technological platforms that can reliably record the AP of excitable cells in a non-invasive manner, at high throughput, and with cost-efficient solutions. The patch clamp technique is the gold standard for accurately recording APs of cells[3]. This method employs a glass micropipette electrode filled with a solution that mimics the ionic composition of the cytosol allowing for the precise intracellular recording of signals from a single cell and enabling the direct measurement of the AP with accurate morphology and duration. While this technique offers precise measurements, it also

[1]Center for Nano Science and Technology, Istituto Italiano di Tecnologia, Milano, Italy. [2]Department of Physics, Politecnico di Milano, Milano, Italy. [3]Istituto Auxologico Italiano IRCCS, Center for Cardiac Arrhythmias of Genetic Origin and Laboratory of Cardiovascular Genetics, Milan, Italy. [4]Plasmon Nano-technologies, Istituto Italiano di Tecnologia, Genova, Italy. [5]Nanoscale Bioelectrical Characterization Group, Institut de Bioenginyeria de Catalunya (IBEC), The Barcelona Institute of Science and Technology (BIST), Barcelona, Spain. [6]Department d'Enginyeria Electrònica i Biomèdica, Universitat de Barcelona, Barcelona, Spain. [7]Department of Biotechnology and Biosciences, University of Milano-Bicocca, Milan, Italy. [8]Present address: School of Electronics and Computer Science, University of Southampton, Southampton SO17 1BJ, UK. [9]These authors contributed equally: Adrica Kyndiah, Giulia Zoe Zemignani ✉e-mail: adrica.kyndiah@iit.it; luca.sala@auxologico.it; mario.caironi@iit.it

comes with drawbacks such as invasiveness, short-term duration of the measurements, post recording cell death, and limited throughput, even after the introduction of automated patch clamp systems[4]. Three-dimensional (3D) micro and nano devices, often combined with electro- or optoporation methods, were proposed to overcome the limitations of patch clamp by enhancing the cell/electrode coupling[5–8]. Similarly, 3D and nanowire transistors have been employed for the recording of APs by physically penetrating the membrane, establishing direct contact with the cell cytoplasm[9–12]. However, the fabrication of nano-porating devices involves a complex manufacturing process, while their inherent invasiveness alters the electrical and contractile properties of the cells. Voltage-sensitive dyes or genetically-encoded voltage indicators allow non-invasive recording of APs, but their use-case is still limited by low sensitivity or technical challenges that require advanced genetic modifications[13,14]. Non-invasive recording of the electrical activity of neurons and cardiomyocytes with higher throughput could be achieved through planar electrodes, with Microelectrode Arrays (MEAs) being the most commonly used technology[15,16]. MEAs probe extracellular field potentials (FPs), with the acquisition of signals with lower information, corresponding to the derivative of APs, affected by noise and various experimental parameters, including the size of the electrode and the cell, and the distance between them, among others[17]. Not all the information contained in the AP can be accurately reconstructed from MEAs readings. To record AP signals with planar electrodes, it is necessary to optoporate or electroporate: such methods are considered minimally invasive compared to patch clamp, yet they require local disruption of the cellular membrane[18–21]. As an alternative to simple electrodes, Field-Effect Transistors (FETs) have been used to record APs, with the aim to leverage signal amplification, local signal processing, and scalability. Current variations with AP shape were recorded non-invasively by means of an insulated gate silicon FET in neurons[22] and cardiac cells[23]. However, owing to a poor cell/transistor seal, most of tested devices recorded FPs, with only less than 20% providing signals with AP morphology, characterized by low signal-to-noise ratio[24]. As an alternative platform, electrolyte-gated FETs made of solution-processable carbon semiconductors were explored for electrophysiological recordings. However, either low-quality shape APs or their derivative could be recorded, as seen for example with poly(3,4-ethylenedioxythiophene)-poly(styrenesulfonate) PEDOT:PSS based organic electrochemical transistors[25–28]. To date, a high throughput method that allows the recording of APs with patch clamp-like quality, without the need of any external physical poration, has not been devised.

Here, we present a platform for the direct recording of cells AP in a non-invasive way with high yield, while meeting the criteria of being easily manufactured and showing promise for scalable fabrication and future high-throughput measurements. Our platform is based on an Electrolyte-Gated Organic Field-Effect Transistor (EGOFET) consisting of a very well-known, prototypical organic semiconducting polymer, regioregular poly(3-hexylthiophene-2,5-diyl) (P3HT), which is deposited by means of cost-effective, sustainable and scalable ink-jet printing[29]. P3HT is currently employed in both organic biosensors and opto-organic biointerfaces applications, including cellular scaffolds, neuronal implants, and actuators for drug release[30–35]. Here, we show that P3HT-based EGOFETs can directly transduce APs with high fidelity from human induced pluripotent stem cell-derived cardiomyocytes (hiPSC-CMs), owing to the spontaneous formation of a high resistance and stable cell/transistor seal junction. The largest amplitude of AP transduced was 50 mV. Notably, AP signals were reliably obtained from nearly all fabricated transistors, across different cell cultures, with a success rate exceeding 90%. We validated our recordings by carrying out a direct comparison with benchmark recordings acquired by patch clamp and MEAs on the same batches of hiPSC-CMs. We investigated the sensitivity of the EGOFET to detect drug-induced AP changes. Remarkably, dynamic changes in the Action Potential Duration (APD) during drug action and subtle oscillations in the AP morphology, such as Early Afterdepolarizations (EADs), were detected, qualifying our approach as a potent tool for advanced high-throughput electrophysiology and heart-on-a-chip applications.

Results and discussion
EGOFET coupled to cardiac cells
A schematic representation of P3HT based EGOFETs is presented in Fig. 1a. A 30-nm-thin film of P3HT was inkjet printed to form the FET channel. The topography of the printed P3HT film reveals a root mean square (r.m.s.) roughness of about 1 nm (Fig. 1b). hiPSC-CM monolayers were then seeded on the fibronectin-coated EGOFETs as shown schematically in Fig. 1c. Previous work demonstrated that neither the prolonged contact with the culturing media nor the sterilization procedure significantly modify the polymer surface morphology[36]. The medium used to maintain the cells in culture acts as the electrolyte of the EGOFET, gated through a platinum electrode. The cells plated on the EGOFET form a monolayer (see Supplementary Movie 1 and Supplementary Fig. S2) and the observed stretched membrane indicates tight cell adhesion (Fig. 1d). The cross-sectional SEM images of hiPSC-CMs plated on the EGOFET (Fig. 1e) display the characteristic morphology of cardiomyocytes. In line with the observed smooth topography of the P3HT layer via AFM, the images further confirm the planar configuration of the cell membrane/P3HT interface within the spatial resolution limits of a few nm.

Action potential recordings
The transfer electrical characteristic curve of EGOFETs in the presence of hiPSC-CMs is reported in Fig. 2a for a drain-source voltage $V_{DS} = -0.5$ V (black curve, left axis), along with the computed transconductance g_m (blue curve, right axis). To record the AP of the cardiac cells, we fixed the source to ground, the voltage difference between the gate and the source (V_{GS}) at -0.8 V, and V_{DS} at -0.5 V, corresponding to a bias point where the transistor is in full accumulation mode, i.e. fully on-state (see output characteristics Supplementary Fig. S3), with a transconductance of ≈40 μS. The recorded drain-source modulated current time trace $\Delta I_{DS}(t)$, is shown in Fig. 2b, black trace. It exhibits a current modulation with an amplitude of 2 μA, the shape in time of which corresponds to a typical cardiac (ventricular-like) AP morphology, and where the frequency of the modulation corresponds to that of cardiac cells contraction (see video in Supplementary S1). The signal-to-noise ratio (SNR) of the EGOFET recording trace shown in Fig. 2b is ~60 dB, given the experimental conditions here adopted. Similar $\Delta I_{DS}(t)$ recording traces obtained from a 3 × 2 array of EGOFET devices on the same chip coupled to the same monolayer is illustrated in Supplementary Fig. S4, and those of various EGOFET devices across different experiments are available in Supplementary Fig. S5. Across 6 independent cell cultures comprising a total of 18 chips, 68 out of 75 EGOFETs successfully recorded signals with AP waveforms, yielding a success rate of 90.7%. In less than 10% of the traces, no AP signal could be observed despite of the presence of the cardiomyocyte monolayer.

To benchmark the quality of the recorded signals acquired by EGOFETs, we compared their recordings with those obtained by two gold-standards: patch clamp (Fig. 2b, blue trace) and commercial MEAs (Fig. 2b, red trace), using hiPSC-CMs from matched batches of differentiation. A zoomed-in view of the signals acquired with the three techniques is shown alongside, where it is already qualitatively evident that EGOFET recordings exhibit similar AP waveform in terms of morphology and duration to those obtained with patch clamp, and differ from those obtained with MEAs, which show the characteristic cardiac field potential morphology. We note that, due to the relatively large area of our EGOFETs, the AP recordings in this case represent an average of signals originating from multiple electrically coupled cells. However, since the patch clamp measurements were also performed
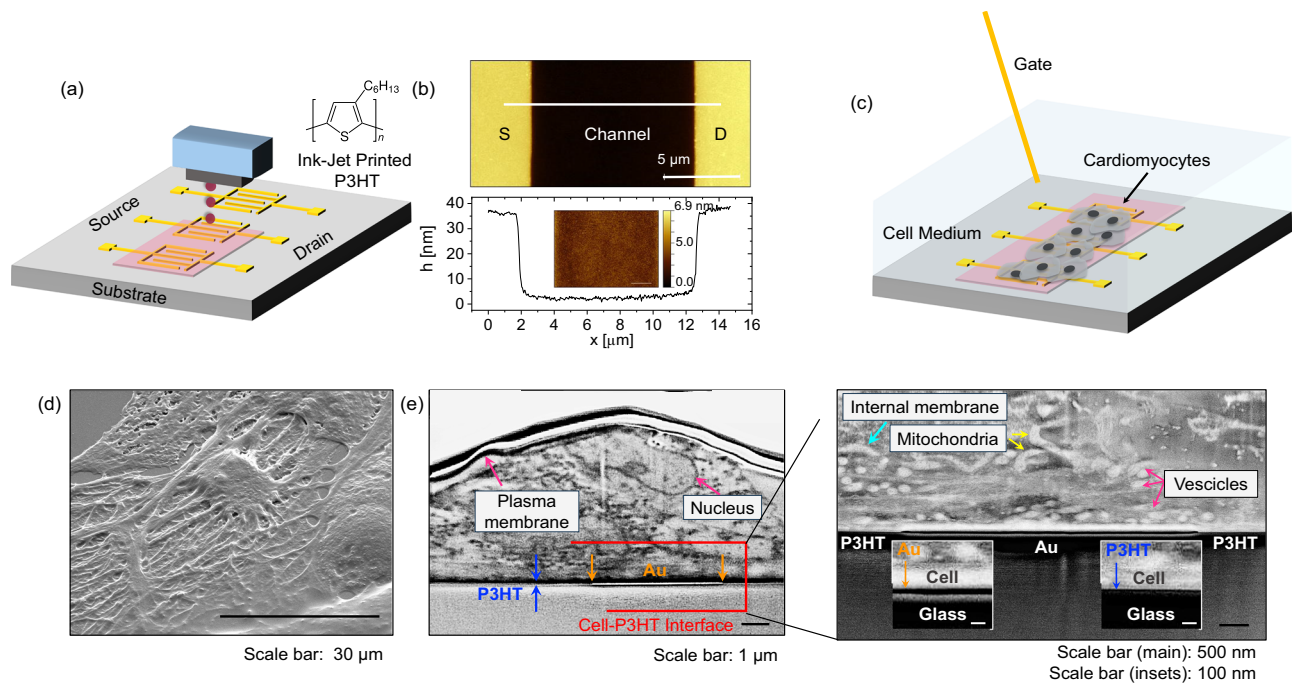
Fig. 1 | Printed EGOFET coupled to cells. a Schematic drawing represents the fabrication of EGOFETs with inkjet printed P3HT. **b** (top) AFM topographic image of the printed P3HT layer covering the source electrode, channel and drain electrode. (below) Line profile of the AFM image taken at the white line. Inset is a zoom of the AFM image in the channel region. **c** Drawing of the EGOFET coupled with the hiPSC-CMs layer, where the cell medium acts as an electrolyte for the EGOFET and a gate electrode made of Pt is immersed into the electrolyte. **d** Top view SEM image of the hiPSC-CMs layer on the EGOFET. **e** SEM image of the cross-section between the cell and the P3HT layer that forms the channel of the EGOFET. The data are representative of cross sections performed on 5 samples obtained from 2 independent cell cultures.

on a monolayer of hiPSC-CMs, the recorded APs do not represent that of a single isolated cell, but rather the activity of an electrically connected network, just probed through the patched cell. While the size of the EGOFET might influence the final SNR, it does not alter the duration, morphology and dynamics of the AP (refer to Supplementary Fig. S6). To quantitatively compare the AP waveform obtained by EGOFETs and patch clamp, we extracted the APD at specific time points during the repolarization phase as a key parameter in evaluating cells electrical activity. In Fig. 2c, we plot the extracted APD_{20}, APD_{50} and APD_{90}, defined as time difference between the AP peak and the timing at which the AP value has decreased by 20%, 50%, 90%, respectively, of the maximum amplitude of the recorded signal by EGOFETs and patch clamp, from at least 6 different sets of cell cultures, and from different sets of devices. The statistical distributions of $APD_{20,}$ APD_{50} and APD_{90} extracted from EGOFETs fall within the range of APDs obtained from patch clamp recordings, with no significant differences as verified with a Student's t test analysis. Additionally, the beating frequency extracted from EGOFETs and patch clamp recordings are notably similar and are in the same range as those obtained from commercial MEAs (Fig. 2d). The direct comparison of signals acquired by the EGOFET platform with those acquired through standard techniques like patch clamp and MEAs validates the EGOFETs ability to capture the main features of APs in a straightforward, non-invasive manner.

Additional tests were conducted to further validate the transducing platform. We examined whether similar recordings could be obtained by altering the fabrication method from inkjet printing to spin-coating technique. As demonstrated in Supplementary Fig. S7, also EGOFETs with spin-coated P3HT exhibited a channel current modulation owing to APs, perfectly in line with the recordings of EGOFETs based on the same inkjet-printed polymer. Next, we changed the configuration of the connections of the EGOFET in such a way that the cell medium is grounded, instead of the source, to mimic the typical conditions of electrophysiological recordings, where the cell bath is normally grounded. The modified bias configuration does not alter the recordings (Supplementary Fig. S8). Results were reproduced in commercial (Fujifilm Cellular Dynamics) and non-commercial (WTC-11 line) hiPSC-CMs (Supplementary Fig. S9).

Transduction mechanism

After validating the recording platform, we shift our focus towards understanding the transduction mechanism between the cardiomyocytes APs and the EGOFET channel current. The periodic variation of $I_{DS}(t)$ over time observed in the EGOFET recordings (Fig. 2b, black curve) indicates that the AP of the cells is changing the effective gate voltage at the cell/semiconductor interface such that:

$$I_{DS}(t) = I'_{DS}(V_{GS}, V_{DS}) + \Delta I_{DS}(t) \qquad (1)$$

where V_{GS} and V_{DS} refers to the gate-source and the drain-source bias voltage applied for AP recording, $\Delta I_{DS}(t) = v_J(t)*g_m$, $v_J(t)$ is the potential at the cleft junction (as shown in Supplementary Fig. S10–1 of SI) that is coupled to the EGOFET, and g_m is the transconductance of the EGOFET at the bias point set during the recording. For the recordings in Fig. 2b, black curve, $g_m = 40\ \mu S$, and $\Delta I_{DS} \approx 2\ \mu A$ at peak (black trace in the representative curve of Fig. 2b), thus leading to an estimated junction cleft voltage amplitude $v_J(t) \approx 50$ mV, which constitutes almost half of the full amplitude of the AP that can be recorded by means of the patch clamp technique ($v_{AP} \approx 100$ mV, blue trace in Fig. 2b). Such value indicates that even if some AP amplitude is lost at the cell/semiconductor interface due to some leakage membrane current, the cleft longitudinal resistance, i.e. the resistance of the cleft in the direction parallel to the transistor surface, is high enough to provide an effective coupling of the cells with the active polymer material (*vide infra*), enabling the transduction of the most relevant features of the AP.
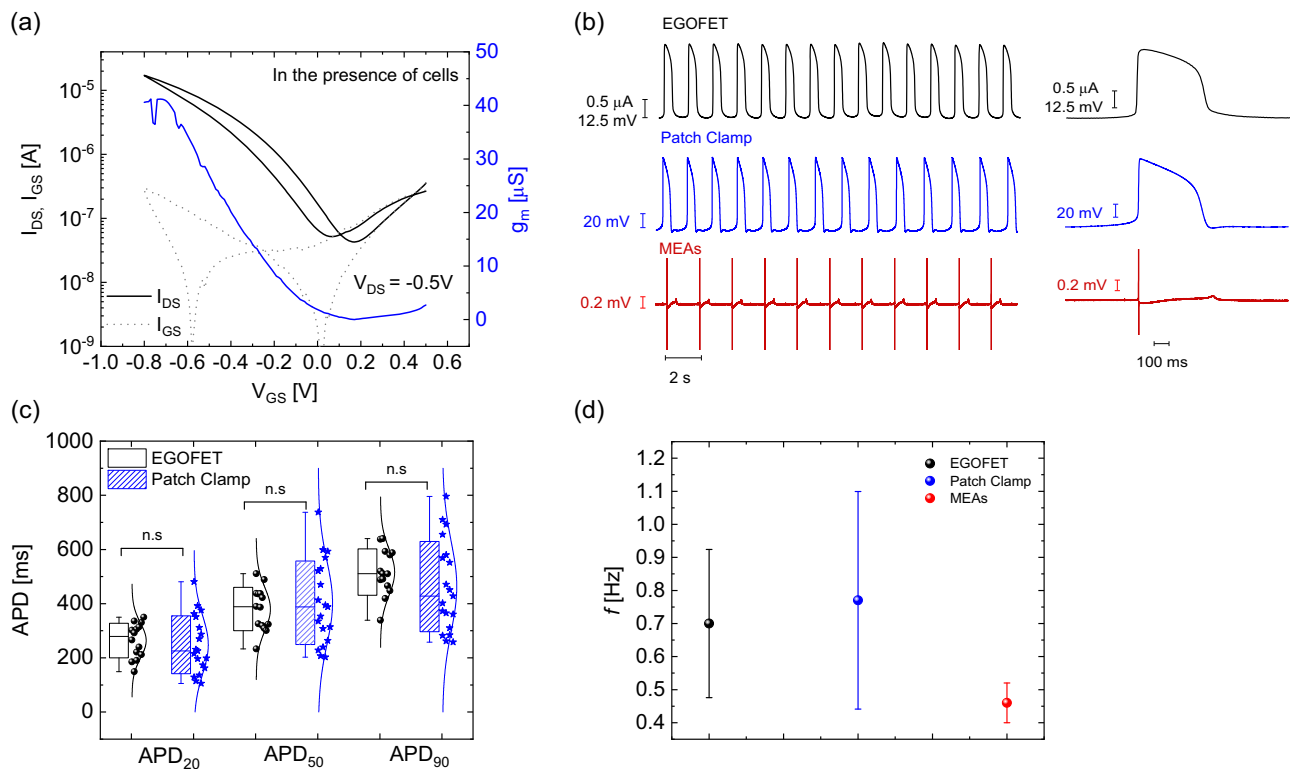
Fig. 2 | Action potentials recording via EGOFETs compared with gold standards in electrophysiology. a Left y-axis: Drain-Source Current I_{DS} (black solid line) and Gate-Source leakage current I_{GS} (gray dashed line) versus Gate-Source Voltage V_{GS} transfer characteristic curves of EGOFETs in electrophysiological condition and in the presence of the hiPSC-CM monolayer. Right y-axis: The blue continuous line is the calculated transconductance from the transfer curve. The interdigitated EGO-FET has a channel length L_{Ch} of 10 μm and channel width W_{Ch} of 19,500 μm. **b** AP recording of the spontaneously beating hiPSC-CMs, where the black trace depicts $\Delta I_{DS}(t)$ versus time recorded at fixed gate and drain voltages: $V_{GS} = -0.8$ V, $V_{DS} = -0.5$ V; blue trace shows the AP recording obtained by patch clamp technique in perforated patch configuration and the red trace is the FP recording obtained from commercial MEAs. **c** APD at 20% (APD_{20}), 50% (APD_{50}) and 90 % (APD_{90}) of the repolarization phase extracted from various EGOFET ($n = 14$) and patch clamp ($n = 19$) traces. Two-sided Student's t test analysis revealed no statistically significant differences in the APDs recorded using EGOFET compared to those obtained via patch clamp. The horizontal lines within the boxes represent the median. The boxes represent 25th and 75th percentiles. Whiskers represent the min-max range. **d** Beating frequency of the AP extracted from EGOFET ($n = 14$), patch clamp ($n = 19$) and from the FP extracted from MEA ($n = 8$) traces.

Equation (1) remains true as long as the transconductance is high enough to disregard the capacitive coupling between cell and transistor. This fact can be directly observed in the recording of the transfer curves by increasing the number of acquired points (i.e. reduced V_{GS} steps down to e.g. 1 mV). The APs modulation become evident in the transfer characteristic curve (Fig. 3a), showing a variation in amplitude and shape as a function of V_{GS} (i.e. of transconductance). Such variation can be observed in the time recorded signals as a function of the bias point in Fig. 3b, which reports the different $I_{DS}(t)$ vs. time recorded traces at different gate voltages, ranging from the fully on-state, $V_{GS} = -0.8$ V, to the off-state, $V_{GS} = +0.2$ V. In the on-state of the transistor, the amplitude of the recorded signal decreases as the gate voltage decreases, as expected due to a decrease in transconductance. In the sub-threshold and off-state region instead (for $V_{GS} < -0.2$ V, dark green trace and for $V_{GS} = 0.2$ V, dark blue trace), the shape of the modulated current signal gets distorted and resembles the derivative of the APs. This is because the transduction in this regime is dominated by the device interfacial capacitance rather than by its transconductance (see Supplementary Fig. S10). The fact that the shape of the AP signals depends on the applied V_{GS} and on the working regime of the transistor further confirms that the electrically active cardiomyocytes interfacing the EGOFET channel are locally acting as a secondary gate superimposed to the bias of the primary gate represented by the platinum electrode: the higher is the transconductance, the higher is the charge density modulation in the accumulated channel due to cells AP, producing a higher modulation of the current.

The transduction of AP signals by the EGOFETs is thus attributed to *i*) the use of an electrolyte gated transistor configuration with sufficiently high transconductance, instead of a simple electrode that would provide capacitive coupling, and *ii*) the formation of an excellent electrical coupling between cardiomyocytes and EGOFETs, with high seal resistance. The latter point can be understood by considering the electrical point contact model approximation described in ref. 37, or its simplified version in ref. 23, adapted to the case of cardiomyocytes.

Theoretical calculations (see Supplementary Figs. S10, S10-1, S10-2) show that with the transistor in the on-state, the current variations recorded by the device match the morphology and duration of APs signals above a critical resistance of the cleft. For lower resistances of the cleft, the current modulation shape is distorted and tends to a field potential like-shape, even if the transistor is kept in the on-state. These results are consistent with the spontaneous formation of a highly resistive cleft between the EGOFET channel and cardiomyocytes, enabling an effective coupling. The latter condition is key to have a large fraction of the transmembrane AP directly modulating the channel conductivity, resulting in high fidelity recording of the AP morphology.

From a phenomenological point of view, we have demonstrated that APs act as gating signals superimposed on the gate bias applied to the device. Since the operation of our device relies on ionic gating, we infer that the ion redistribution occurring during an AP transiently modifies the local electrochemical potential, modulating the polymer channel conductivity. We rationalize the observed phenomenon in
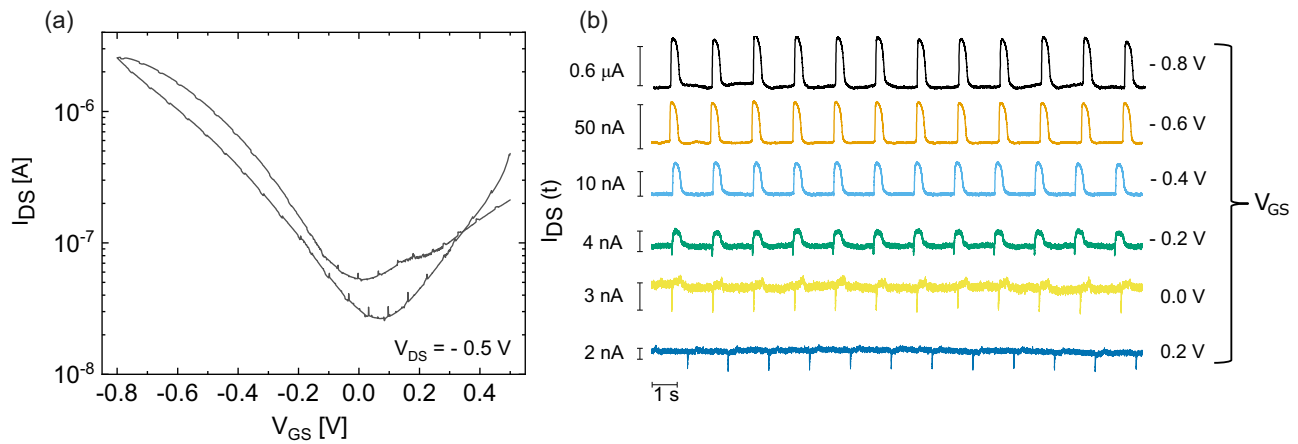
Fig. 3 | Action potential recorded at different gate bias point. a Source-Drain Current I_{DS} versus Gate-Source Voltage V_{GS} transfer characteristic curves of the EGOFETs, manifesting the dynamic AP modulation superimposed to the static curve. V_{GS} was swept from 0.5 V to −0.8 V in steps of 1 mV, while $V_{DS} = −0.5$ V. **b** Transistor current trace ΔI_{DS} recorded at different V_{GS} ranging from a full on-state ($V_{GS} = −0.8$ V, black trace) to the off-state ($V_{GS} = 0.2$ V, dark blue trace) in steps of 0.2 V.

terms of an excellent coupling of the membrane with the active channel of our device, leading to the formation of a highly resistive cleft. This is supported by our calculations, based on a point contact model adapted to Luo-Rudy cardiac model, which indicates that, besides a good transconductance, the field generated by the redistribution of ions during an AP can be effectively coupled to the transistor only if the seal impedance is sufficiently high. The reason that leads to such an effective coupling will require further extensive investigations, stimulated by our foundational findings. While the smooth morphology observed in Fig. 1b may contribute to the formation of such a tight cleft, surface flatness alone is unlikely to fully account for the strong coupling observed. Other factors, comprising the surface energy of the polymer and its mechanical properties can play a role, and shall be systematically investigated in future experiments.

Drug tests

Pharmacological screening of drug effects on cardiomyocytes is generally performed by monitoring the shape and duration of FPs or APs. To evaluate the efficacy and the versatility of our EGOFET technology in safety pharmacology screenings, we dynamically monitored the effect of the APD-shortening drug Nifedipine (NIFE) and the APD-prolonging drug E-4031. NIFE is a selective calcium channel blocker that specifically targets L-type calcium channels, reducing the entry of calcium ions into the cells during the AP and leading to a decrease in the APD of cardiomyocytes[38]. Figure 4a represents the baseline current recording before the application of drugs. On this culture, 1 μM NIFE was added to the cell medium during the recording (Fig. 4b), and multiple signal acquisitions were carried out after administration (Fig. 4c, d). Before the drug administration, the electrical current signals have the same distinctive AP morphology of a ventricular-like hiPSC-CM, as seen in the overlapped signals in Fig. 4e. Once NIFE was administered, the APD starts to progressively shorten over time, as illustrated by the overlapped signals in Fig. 4f. The shortening of the APD stabilizes with time, indicating that a steady-state was reached, and diastolic oscillations become evident (Fig. 4g, h). Next, we tested the effect of the APD-prolonging drug E-4031, a selective hERG channel blocker that induces AP prolongation and potentially triggers drug-induced arrhythmias promoting the formation of Early After Depolarizations (EADs). Figure 4i illustrates the recordings of the baseline before adding E-4031. Subsequently, the recordings in Fig. 4j indicate the gradual APD prolongation, a visible repolarization instability and the progressive change in the current contour expected from a hERG blocker. Remarkably evident EADs and APD alternans were recorded,

as visible in Fig. 4k, marked with alternating black and red circles above the signals. Persistent EADs with minor AP plateau oscillations were visible and recorded at the steady state with E-4031, as visible in Fig. 4l. The total recording time to monitor the effect of both drugs with the EGOFET platform is about 30 min. The effect of both NIFE and E-4031 on the APD of a similar cell culture was further validated with the standard patch clamp technique, as shown in Supplementary Fig. S11. In the case of patch clamp, the total recording time could not exceed 10 min due to the challenges in maintaining a high-quality seal in contracting monolayers of hiPSC-CMs, thus preventing longer recordings.

In conclusion, we have presented an in vitro electrophysiological tool based on scalable printed electrolyte-gated polymer transistors for spontaneous and non-invasive recording of AP from cardiomyocytes. The signal quality is comparable to that of gold-standard patch clamp technique, while stability is improved, enabling consecutive recordings and extended measurement duration up to 30 min. The AP recordings were obtained by measuring the AP modulation of transistor channel current when it is in accumulation regime, without the need of any external poration stimuli. Our findings were validated by directly comparing AP signals recorded via EGOFETs with those from standard patch clamp technique and commercial MEAs. The EGOFETs based transducing platform was assessed as a tool in drug tests on hiPSC-CMs to monitor the effect of APD-shortening drug NIFE and of the APD-prolonging drug E-4031. The EGOFET platform has comparable sensitivity to patch clamp in detecting AP shape, EADs and diastolic instability, while significantly outclasses MEAs in recording quality and sensitivity in detecting EADs or diastolic oscillations. Being non-invasive, it offers higher reliability and reproducibility compared to poration techniques. The high yield of the approach and simplicity in operating the device will offer electrophysiologists a scalable tool to stably record AP in future applications with precise morphology, increased throughput compared to patch clamp and without perturbing cells through transient electrical or optical poration. While APs with higher SNR are achieved at maximum V_{GS}, potential disruption of the membrane post-recording may occur, limiting the ability to record from the same cells over multiple days. Therefore, the operational window for AP recordings should be carefully selected to maximize transconductance without applying excessively high voltages (Supporting Information SI 12). Our findings contribute toward the recent Food and Drug Administration F.D.A. Modernization Act 2.0 that emphasizes the use of alternative in vitro electrophysiological tools for preclinical trials of newly discovered drugs. This system can be easily integrated into heart-on-chip applications for long term- and high-
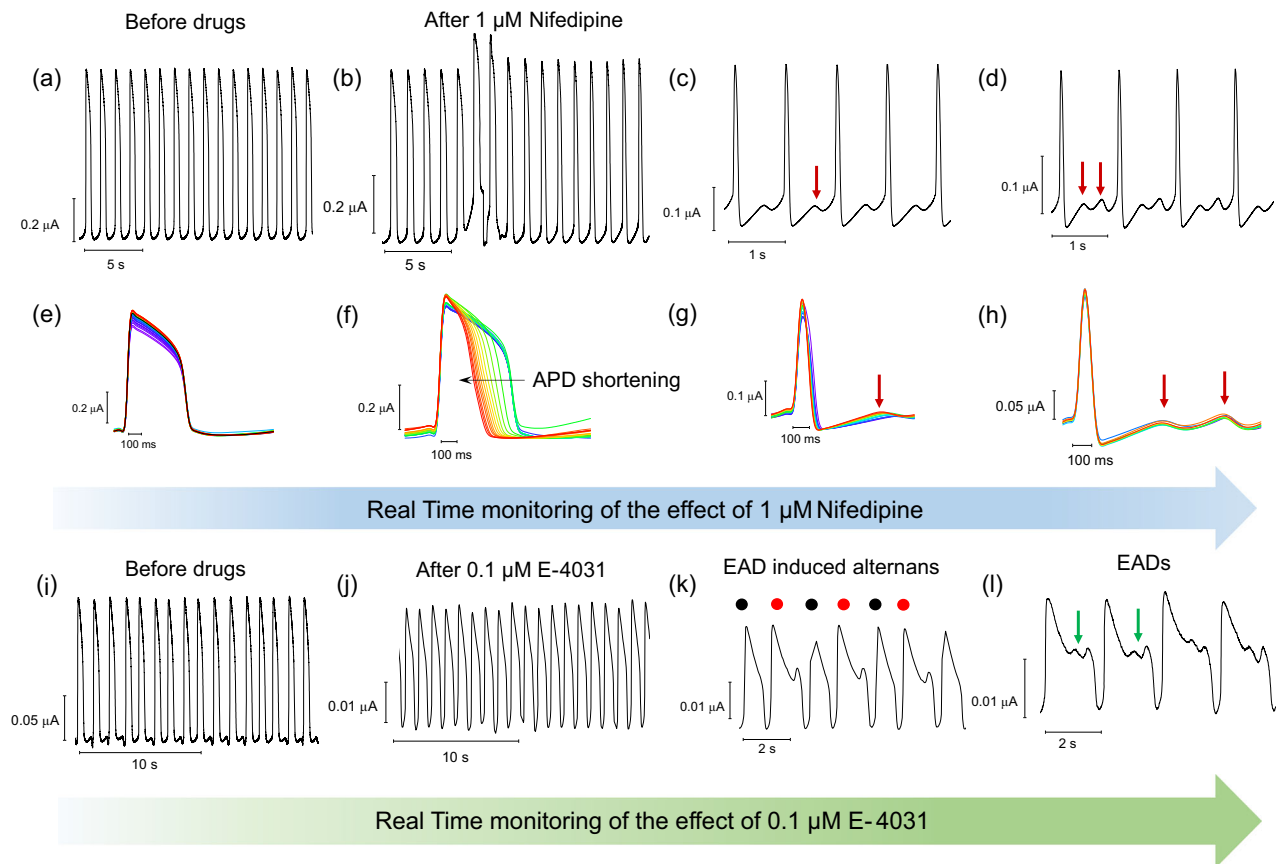
Fig. 4 | Non-invasive drug screening application of EGOFETs with hiPSC-CMs.
a Baseline recording of the hiPSC-CM monolayers prior to the addition of NIFE.
b Current recording trace after administration of 1 μM of NIFE; **c** and **d** are recording
traces of hiPSC-CMs after the administration of NIFE. **e** Overlapped AP signals of
recording trace (**a**). **f** Overlapping the signals from recording trace (**b**), depicting
the dynamic change of the AP morphology after adding NIFE. **g** and **h** are over-
lapped AP signals from recording traces (**c**) and (**d**), respectively. Red arrows in (**c**),
(**d**), (**g**) and (**h**) indicate the diastolic oscillations. **i** Baseline recording of cells before
adding E-4031. **j** Current recording trace after the addition of 0.1 μM of E-4031.
k, l Consecutive recordings after adding E-4031 to monitor its effect. Black and red
circles in panel (**k**) mark the alternated AP morphology commonly called EAD-
induced-alternans, which indicate clear pro-arrhythmic events. Green arrows in (**l**)
indicate EADs.

quality recordings of electrical activities with virtually any cardiac
disorders. Beyond cardiac applications, this platform holds promise in
the study of other electrogenic cells such as neurons and smooth or
skeletal muscle cells.

Methods
Ethics
This study does not involve experiments involving animals, human
participants, or clinical samples. hiPSCs were purchased from the
Coriell Institute and appropriate Material Transfer Agreements were
signed.

EGOFET electrodes fabrication
To fabricate the source and drain electrodes of EGOFET devices,
corning glass substrates (700 μm thick) were chosen to ensure stabi-
lity, robustness and biocompatibility to the cardiac cell culture. The
source and drain electrodes were fabricated by means of a mask-less
image reversal lithography process. After a cleaning step via oxygen
plasma, a layer of photoresist (AZ5214E) was spin-coated on top of the
substrate for 60 s at 4000 rpm, followed by a baking step at 110 °C for
90 s. Following the evaporation of the solvent, the sample was nega-
tively exposed using an MLA100 Heidelberg mask-less aligner. The
successive baking at 120 °C for 90 s and UV exposure guaranteed the
complete crosslinking of the non-exposed areas. Development in
AZ726MIF revealed the desired pattern which was then coated with
2 nm of chromium and 30 nm of gold by thermal evaporation. The final

lift-off step in Technistrip Micro-D2 provided interdigitated source-
drain electrodes with selected features (L_{Ch} = 10 μm; W_{Ch} = 19,500 μm).

P3HT printing
To avoid the exposure of gold leads to the electrolyte environment,
some parts of the transistors (excluding the channel) were passivated
by ink-jet printing of a biocompatible insulator (SU8 – TF6001) using a
Fujifilm Dimatix DMP-2831. Subsequently, the printed pattern was
crosslinked by 120 °C baking for 15 min and UV flood exposure. The
active material, poly(3-hexylthiophene-2,5-diyl) (P3HT) organic semi-
conductor, was ink-jet printed on the channel of our transistors. We
used a custom-made solution of regioregular P3HT in a blend of ortho-
dichlorobenzene (ODCB) and chlorobenzene (CB) in a ratio of 25/75
ODCB/CB with a concentration of 2.6 mg/mL, which was specifically
optimized to be printed at a substrate temperature of 35 °C with a drop
spacing of 45 μm. These parameters ensured high on/off ratio,
minimal hysteresis and effective reproducibility of the samples. At last,
a 3D printed custom-made well of black PLA was attached on our
sample to confine the electrolyte on the transistors by using a
biocompatible glue.

hiPSC culture and differentiation towards hiPSC-CMs
Bona fide healthy hiPSCs were obtained from the Coriell Institute for
Medical Research (deposited identifier GM25256) from the WTC-11
hiPSC line (hPSCReg UCSFi001-A) with appropriate Material Transfer
Agreement.

HiPSCs were cultured on multiwell plates coated with recombinant human vitronectin (rhVTN, Thermo Fisher Scientific) in E8 Flex medium (Thermo Fisher Scientific). HiPSCs were replated on hESC qualified Matrigel matrix (BD Biosciences) before cardiac differentiation and differentiated to hiPSC-derived cardiomyocytes following a protocol based on the modulation of the Wnt-signaling pathway[39]. HiPSC-CMs were purified through glucose starvation (final purity >90% CMs) as earlier described[40] and cryopreserved on day 9–16. For each experiment, cryopreserved hiPSC-CMs were thawed and expanded by addition of 4 μM CHIR99021 (SelleckChem) to the culture medium according to a previously published protocol[41]. hiPSC-CMs were maintained in RBK1 medium consisting of RPMI1640 medium (Euroclone) supplemented with B27 Supplement and 1% KnockOut Serum Replacement (Thermo Fisher Scientific).

Cell plating on the EGOFETs
EGOFETs were sterilized by consequently washing them with water, 70% ethanol and 100% ethanol (repeated twice) and then air dried for 5 min. The channel area was coated with 40 μg/mL bovine fibronectin solution in PBS (Merck) for 1 h in a humidified atmosphere at 37 °C. Identical coating procedures were performed for MEAs and transistors, with the sole adaptation of the working volume for the surface area. The same cell density of 500.000 cells/cm² as for MEAs was used for plating. Fibronectin solution was removed and cells were seeded in a 10 μL drop of RBK1 medium supplemented with Revitacell (Thermo Fisher Scientific). Cell drops were incubated for 1 h in a humidified atmosphere at 37 °C, 5% CO₂ to make cell monolayer form on top of the transistor. Then, 300 μL of RBK1 medium supplemented with Revitacell was added to the chamber and transistors were incubated in a humidified atmosphere at 37 °C, 5% CO₂. Next day and twice a week thereafter 60% of the medium was refreshed with RBK1.

EGOFET recordings
The EGOFET characterization and action potential recordings were carried out using the Agilent B2912A source meter. Prior to the AP recordings, the EGOFETs containing the living cells were electrically characterized by taking a transfer curve (I_{DS} versus V_{GS}) where we sweep V_{GS} from +0.5 V to −0.8 V in steps of 0.01 V, keeping V_{DS} constant at −0.5 V. Transconductance g_m is then extracted from the transfer curve by taking the first derivative, i.e. $g_m = \partial I_{DS}/\partial V_{GS}$. A Pt Wire 99.99+ % Hard, with a 0.5 mm diameter was purchased from Advent Research Materials and used as the gate electrode. To record the APs, we recorded the $I_{DS}(t)$ at fixed V_{GS} and V_{DS} over time at sampling rate of 10 kHz. Data analysis of the current traces involved only the subtraction of the baseline to correct the drift of $I_{DS}(t)$ over time. The baseline subtraction was done in *Origin 2018* → Peak Analyser → Baseline Mode → Asymmetric Least Squares Smoothing Baseline.

Drug tests
Nifedipine (Merck) stock solution was prepared in DMSO to a concentration of 10 mM and used at a final concentration of 1 μM in culture medium. E4031 (Tocris) was dissolved in water to create a stock solution with a concentration of 10 mM. A final concentration of 0.1 μM in culture medium was used. For monitoring of the effect of drugs in real time, 7 μL of each drug was added to the pool during the EGOFET AP recordings.

Multielectrode arrays recording
Multiwell MEAs (24 wells, MultiChannel Systems) with gold electrodes on FR4 epoxy were coated with 40 μg/mL bovine fibronectin solution in PBS (Merck) and processed as previously described[42]. hiPSC-CMs were dissociated with TrypLE Select 10X (Thermo Fisher Scientific) and replated on Multiwell MEAs as confluent monolayers. RBK1 medium

was refreshed every 48–72 h. Identical coating procedures were performed for MEAs and EGOFETs, with the sole adaptation of the working volume for the surface area. The monolayer density of 500.000 cells/cm² was used in both conditions.

MEAs recordings were achieved through a dedicated instrument, i.e. the Multichannel Systems 24-well Multiwell MEA system, using hiPSC-CMs obtained from the same differentiation(s) as those plated on EGOFETs. HiPSC culture, hiPSC-CM differentiation and plating were done in parallel on both EGOFETs and MEAs. The recordings were conducted separately due to logistic limitations. The diameter of the MEA electrodes, in our configuration, is 100 μm. MEA electrodes have a 700 μm spacing. MEA recordings were acquired at 10 kHz and filtered through high-pass and low-pass filters (Bessel) at 1 Hz and 3.5 kHz correspondingly.

Patch clamp recordings
hiPSC-CMs were plated in monolayer (80.000 cells) for patch clamp measurements on ink jet printed P3HT film coated with 40 μg/mL bovine fibronectin solution in PBS (Merck). APs were recorded with perforated patch clamp technique using pore-forming antibiotic amphotericin B (0.22 mM dissolved in dimethyl sulfoxide, DMSO) at physiological temperature (37 °C). The recordings were performed in current clamp configuration ($I = 0$). Pipette was filled with an intracellular solution contained (in mM): 110 K-aspartate, 23 KCl, 3 MgCl₂, 0.04 CaCl₂, 0.1 EGTA KOH (10⁻⁷ M free-Ca²⁺), 5 HEPES KOH, 0.4 Na+-GTP, 5 Na+-ATP, 5 Na+-phosphocreatine, pH adjusted to 7.3 with KOH. The extracellular solution consisted in (mM): 137 NaCl, 5.4 KCl, 2 CaCl₂, 1 MgCl₂, 10 Hepes, 10 Glucose, pH adjusted to 7.4 with NaOH. Powders were all purchased from Merck.

Digidata (1440A) and Multiclamp (700B) (Axon Instruments) coupled with an upright microscope (Olympus BW63) were employed to perform patch clamp experiments. Data were acquired with the pCLAMP10 software (Axon Instruments) and then analyzed with Clampfit (Axon Istruments) and Origin 8.0 (OriginLab Corporation).

Scanning electron microscopy-focused ion beam (SEM-FIB)
Cell fixing. Samples were fixed in a solution of 2% Glutaraldehyde in 0.1 M Cacodylate buffer for 1.5 h at room temperature, and post-fixed in 1% osmium tetroxide in 0.1 M Cacodylate buffer for 2 h. After three washes in MQ H₂O, the samples were dehydrated in rising concentrations of ethanol solutions (from 30% to 100%), 1:1 ethanol:hexamethyldisilazane (HMDS, Sigma-Aldrich) and 100% HMDS, and air-dried overnight.

Cell cross sectioning. Cross-sectional imaging was conducted on previously fixed samples, using a SEM/FIB Dual Beam system (Helios Nanolab 650, FEI). Prior to imaging, the samples were coated with a 10 nm Au thin film (Sputter Coater system KS500 Confocal, Kenosistec s.r.l.). A region of interest was identified by imaging the sample under electron beam irradiation at 3 kV and 83 pA. An additional conductive layer of platinum, 100-nm thin, was deposited by electron beam-assisted deposition (tilt: 0 degrees, 3 kV, 83 pA), followed by a 900-nm thick layer deposited on the tilted sample (52 degrees) via ion beam-assisted deposition. The Pt layer was necessary to yield fine cutting and observe internal cellular structures at high resolution. Cross sectioning was performed in two steps. First, an area of 30 μm × 30 μm positioned in front of the cell was excavated at currents of 65 nA (high currents). These allowed to free the space in front of the cell of interest, as needed for consequent imaging. The cell was then cut in two steps at lower currents: the first larger cut was performed at 45 pA to remove almost half of the cell surface, followed by a finer cut at 18 pA for final observation of the central area. Cells sectional images were then acquired by electron beam in immersion mode at 52 degrees tilt, 3 k V, 43 pA.

Atomic force microscopy (AFM)

AFM measurements were performed at about 25 °C, in air, using a Dimension Icon (Bruker) AFM microscope. PPP-FMAuD cantilevers (spring constant $\cong$ 2 N·m^{-1}, frequency $\cong$ 150 kHz) were used for standard tapping mode imaging. AFM images were flattened by means of Gwyddion (www.gwyddion.net).

Statistical analysis

For the analysis in Fig. 2c, normality was assessed using the Shapiro–Wilk test, which confirmed that all data groups followed a normal distribution. A two-tailed unpaired t-test revealed no significant difference between groups ($P > 0.05$). Figure 2d presents the mean values, with error bars representing the standard deviation.

Reporting summary

Further information on research design is available in the Nature Portfolio Reporting Summary linked to this article.

Data availability

All data supporting the findings of this study are available within the article and its supplementary files. Any additional requests for information can be directed to, and will be fulfilled by, the corresponding authors.

References

1. Hong, G. & Lieber, C. M. Novel electrode technologies for neural recordings. *Nat. Rev. Neurosci.* **20**, 330–345 (2019).
2. Varró, A. et al. Cardiac transmembrane ion channels and action potentials: cellular physiology and arrhythmogenic behavior. *Physiol. Rev.* **101**, 1083–1176 (2021).
3. Sakman, B. & Neher, E. Patch clamp techniques for studying ionic channels in excitable membranes. *Ann. Rev. Physiol.* **46**, 455–472 (1984).
4. Seibertz, F. et al. A modern automated patch-clamp approach for high throughput electrophysiology recordings in native cardiomyocytes. *Commun. Biol.* **5**, 1–10 (2022).
5. Jahed, Z. et al. Nanocrown electrodes for parallel and robust intracellular recording of cardiomyocytes. *Nat. Commun.* **13**, 1–14 (2022).
6. Dipalo, M. et al. Intracellular and extracellular recording of spontaneous action potentials in mammalian neurons and cardiac cells with 3D plasmonic nanoelectrodes. *Nano Lett.* **17**, 3932–3939 (2017).
7. Capozza, R. et al. Cell membrane disruption by vertical micro-/nanopillars: role of membrane bending and traction forces. *ACS Appl. Mater. Interfaces* **10**, 29107–29114 (2018).
8. Desbiolles, B. X. E. et al. Nanovolcano microelectrode arrays: toward long-term on-demand registration of transmembrane action potentials by controlled electroporation. *Microsyst. Nanoeng.* **6**, 67 (2020).
9. Duan, X. et al. Intracellular recordings of action potentials by an extracellular nanoscale field-effect transistor. *Nat. Nanotechnol.* **7**, 174–179 (2012).
10. Kruskal, P. B., Jiang, Z., Gao, T. & Lieber, C. M. Beyond the patch clamp: nanotechnologies for intracellular recording. *Neuron* **86**, 21–24 (2015).
11. Zhao, Y. et al. Scalable ultrasmall three-dimensional nanowire transistor probes for intracellular recording. *Nat. Nanotechnol.* **14**, 783–790 (2019).
12. Gu, Y. et al. Three-dimensional transistor arrays for intra- and intercellular recording. *Nat. Nanotechnol.* **17**, 292–300 (2022).
13. Miller, E. W. et al. Optically monitoring voltage in neurons by photoinduced electron transfer through molecular wires. *Proc. Natl Acad. Sci. USA* **109**, 2114–2119 (2012).
14. Yang, H. H. & St-Pierre, F. Genetically encoded voltage indicators: opportunities and challenges. *J. Neurosci. J. Soc. Neurosci.* **36**, 9977–9989 (2016).
15. Spira, M. E. & Hai, A. Multi-electrode array technologies for neuroscience and cardiology. *Nat. Nanotechnol.* **8**, 83–94 (2013).
16. Sala, L., Ward-van Oostwaard, D., Tertoolen, L. G. J., Mummery, C. L. & Bellin, M. Electrophysiological analysis of human pluripotent stem cell-derived cardiomyocytes (hPSC-CMs) using multielectrode Arrays (MEAs). *J. Vis. Exp.* https://doi.org/10.3791/55587 (2017).
17. Plonsey, R. & Barr C., R. *Bioelectricity A Quantitative Approach*. https://doi.org/10.1007/978-0-387-48865-3. (2007).
18. Tertoolen, L. G. J., Braam, S. R., van Meer, B. J., Passier, R. & Mummery, C. L. Interpretation of field potentials measured on a multi electrode array in pharmacological toxicity screening on primary and human pluripotent stem cell-derived cardiomyocytes. *Biochem. Biophys. Res. Commun.* **497**, 1135–1141 (2018).
19. Melle, G. et al. Intracellular recording of human cardiac action potentials on market-available multielectrode array platforms. *Front. Bioeng. Biotechnol.* **8**, 1–10 (2020).
20. Dipalo, M. et al. Plasmonic meta-electrodes allow intracellular recordings at network level on high-density CMOS-multi-electrode arrays. *Nat. Nanotechnol.* **13**, 965–971 (2018).
21. Dipalo, M. et al. Intracellular action potential recordings from cardiomyocytes by ultrafast pulsed laser irradiation of fuzzy graphene microelectrodes. *Sci. Adv.* **7**, 1–10 (2021).
22. Fromherz, P., Offenhausser, A. & Vetrrer, T. A neuron-silicon junction: a Retzius cell of the leech on an insulated-gate field-effect transistor. *Science* **252**, 1290–1293 (1991).
23. Sprössler, C., Denyer, M., Britland, S., Knoll, W. & Offenhäusser, A. Electrical recordings from rat cardiac muscle cells using field-effect transistors. *Phys. Rev. E Stat. Phys. Plasmas Fluids Relat. Interdiscip. Top.* **60**, 2171–2176 (1999).
24. Steinhoff, G. et al. Recording of cell action potentials with AlGaN-GaN field-effect transistors. *Appl. Phys. Lett.* **86**, 1–3 (2005).
25. Kyndiah, A. et al. Bioelectronic recordings of cardiomyocytes with accumulation mode electrolyte gated organic field effect transistors. *Biosens. Bioelectron.* **150**, 111844 (2020).
26. Kyndiah, A. et al. Direct recording of action potentials of cardiomyocytes through solution processed planar electrolyte-gated field-effect transistors. *Sens. Actuators B Chem.* **393**, 134227 (2023).
27. Hempel, F. et al. PEDOT:PSS organic electrochemical transistor arrays for extracellular electrophysiological sensing of cardiac cells. *Biosens. Bioelectron.* **93**, 132–138 (2017).
28. Gu, X., Yao, C., Liu, Y. & Hsing, I. M. 16-Channel organic electrochemical transistor array for in vitro conduction mapping of cardiac action potential. *Adv. Healthc. Mater.* **5**, 2345–2351 (2016).
29. Blasi, D. et al. Printed, cost-effective and stable poly(3-hexylthiophene) electrolyte-gated field-effect transistors. *J. Mater. Chem. C.* **8**, 15312–15321 (2020).
30. Ghezzi, D. et al. A polymer optoelectronic interface restores light sensitivity in blind rat retinas. *Nat. Photonics* **7**, 400–406 (2013).
31. Milos, F. et al. High aspect ratio and light-sensitive micropillars based on a semiconducting polymer optically regulate neuronal growth. *ACS Appl. Mater. Interfaces* **13**, 23438–23451 (2021).
32. Genco, E. et al. Single-molecule bioelectronic portable array for early-diagnosis of pancreatic cancer precursors. *Adv. Mater.* **35**, 2304102 (2023).
33. Aziz, I. A., Tullii, G. & Antognazza, M. R. Poly(3-hexylthiophene) as a versatile semiconducting polymer for cutting-edge bioelectronics. *Mater. Horizons* https://doi.org/10.1039/d5mh00096c (2025).
34. Chiaravalli, G., Manfredi, G., Sacco, R. & Lanzani, G. Photoelectrochemistry and Drift-Diffusion Simulations in a Polythiophene Film

Interfaced with an Electrolyte. *ACS Appl. Mater. Interfaces* **13**, 36595–36604 (2021).

35. Chiaravalli, G. et al. The light-dependent pseudo-capacitive charging of conjugated polymer nanoparticles coupled with the depolarization of the neuronal membrane. *Phys. Chem. Chem. Phys.* **26**, 47–56 (2023).

36. Vaquero, S. et al. Conjugated polymers for the optical control of the electrical activity of living cells. *J. Mater. Chem. B* **4**, 5272–5283 (2016).

37. Schätzthauer, R. & Fromherz, P. Neuron-silicon junction with voltage-gated ionic currents. *Eur. J. Neurosci.* **10**, 1956–1962 (1998).

38. Charnet, P., Ouadid, H., Richard, S. & Nargeot, J. Electrophysiological analysis of the action of nifedipine and nicardipine on myocardial fibers. *Fundam. Clin. Pharmacol.* **1**, 413–431 (1987).

39. Lian, X. et al. Robust cardiomyocyte differentiation from human pluripotent stem cells via temporal modulation of canonical Wnt signaling. *Proc. Natl. Acad. Sci. USA.* **109**, E1848-57 (2012).

40. Tohyama, S. et al. Distinct metabolic flow enables large-scale purification of mouse and human pluripotent stem cell-derived cardiomyocytes. *Cell Stem Cell* **12**, 127–137 (2013).

41. Buikema, J. W. et al. Wnt activation and reduced cell-cell contact synergistically induce massive expansion of functional human iPSC-derived cardiomyocytes. *Cell Stem Cell* **27**, 50–63.e5 (2020).

42. Sala, L., Ward-Van Oostwaard, D., Tertoolen, L. G. J., Mummery, C. L. & Bellin, M. Electrophysiological analysis of human pluripotent stem cell-derived cardiomyocytes (hPSC-CMs) using multielectrode arrays (MEAs). *J. Vis. Exp.* **2017**, 1–15 (2017).

Acknowledgements

Author contributions

A.K. and M.C. conceived and designed the experiments. G.Z. fabricated the EGOFETs. F.V. optimized the printing process. Cardiomyocytes were cultured and plated in P.J.S.'s lab by L.S. and A.Kh.. C.R. and G.T. carried out the patch clamp measurements under the supervision of M.R.A.. L.S. and A.Kh. carried out all the MEA recordings. R.M. performed and analyzed the SEM-FIB cross section images under the supervision of F.D.A. G.I. cultured the commercial cells. S.C. wrote the python script for the analysis of the recording traces. G.G. worked on the theoretical investigation of the transistor/cell coupling. L.S. coordinated all the parts related to cell culture and drug testing. A.K. and G.Z. carried out all EGOFET recordings. A.K. carried out the data analysis. A.K. wrote the manuscript with inputs from all the authors. A.K. and M.C. supervised and managed the project.

Competing interests

The authors declare no competing interests.

Additional information

Supplementary information The online version contains supplementary material available at https://doi.org/10.1038/s41467-025-63484-1.

Correspondence and requests for materials should be addressed to Adrica Kyndiah, Luca Sala or Mario Caironi.

Peer review information *Nature Communications* thanks the anonymous reviewers for their contribution to the peer review of this work. A peer review file is available.

Reprints and permissions information is available at http://www.nature.com/reprints

Publisher's note Springer Nature remains neutral with regard to jurisdictional claims in published maps and institutional affiliations.